Retinal Phenotyping of Ferrochelatase Mutant Mice Reveals Protoporphyrin Accumulation and Reduced Neovascular Response

S. P. B. Sardar Pasha,[1,*] Trupti Shetty,[1,2] Nathan A. Lambert-Cheatham,[1] Kamakshi Sishtla,[1] Deepa Mathew,[1] Anbukkarasi Muniyandi,[1] Neeta Patwari,[1] Ashay D. Bhatwadekar,[1,2] and Timothy W. Corson[1–3]

[1]Eugene and Marilyn Glick Eye Institute, Department of Ophthalmology, Indiana University School of Medicine, Indianapolis, Indiana, United States
[2]Department of Pharmacology and Toxicology, Indiana University School of Medicine, Indianapolis, Indiana, United States
[3]Department of Biochemistry and Molecular Biology, Indiana University School of Medicine, Indianapolis, Indiana, United States

Correspondence: Timothy W. Corson, Eugene and Marilyn Glick Eye Institute, 1160 West Michigan Street, Indianapolis, IN 46202, USA; tcorson@iu.edu.

SPBSP and TS contributed equally to the work presented here.

Current address: *Department of Cell Biology and Human Anatomy, University of California Davis, Davis, California, United States.

Received: November 11, 2020
Accepted: February 1, 2021
Published: February 23, 2021

Citation: Sardar Pasha SPB, Shetty T, Lambert-Cheatham NA, et al. Retinal phenotyping of ferrochelatase mutant mice reveals protoporphyrin accumulation and reduced neovascular response. *Invest Ophthalmol Vis Sci.* 2021;62(2):36. https://doi.org/10.1167/iovs.62.2.36

Purpose. Heme depletion, through inhibition of ferrochelatase (FECH), blocks retinal and choroidal neovascularization. Both pharmacologic FECH inhibition and a partial loss-of-function *Fech* mutation (*Fech*^{m1Pas}) are associated with decreased neovascularization. However, the ocular physiology of *Fech*^{m1Pas} mice under basal conditions has not been characterized. Here, we aimed to characterize the retinal phenotype of *Fech*^{m1Pas} mice.

Methods. We monitored retinal vasculature at postnatal day 17, 2 months, and 6 months in *Fech*^{m1Pas} homozygotes, heterozygotes, and their wild-type littermates. We characterized *Fech* substrate protoporphyrin (PPIX) fluorescence in the eye (excitation = 403 nm, emission = 628 nm), retinal function by electroretinogram, visual acuity by optomotor reflex, and retinal morphology by optical coherence tomography and histology. We stained vasculature using isolectin B4 and fluorescein angiography. We determined endothelial sprouting of retinal and choroidal tissue ex vivo and bioenergetics of retinal punches using a Seahorse flux analyzer.

Results. Fundi, retinal vasculature, venous width, and arterial tortuosity showed no aberrations. However, VEGF-induced retinal and choroidal sprouting was decreased in *Fech*^{m1Pas} mutants. Homozygous *Fech*^{m1Pas} mice had pronounced buildup of PPIX in the posterior eye with no damage to visual function, bioenergetics, and integrity of retinal layers.

Conclusions. Even with a buildup of PPIX in the retinal vessels in *Fech*^{m1Pas} homozygotes, the vasculature remains normal. Notably, stimulus-induced ex vivo angiogenesis was decreased in *Fech*^{m1Pas} mutants, consistent with reduced pathologic angiogenesis seen previously in neovascular animal models. Our findings indicate that *Fech*^{m1Pas} mice are a useful model for studying the effects of heme deficiency on neovascularization due to *Fech* blockade.

Keywords: ferrochelatase, heme, phenotype, vasculature, mutation

Ferrochelatase (FECH) catalyzes heme production in the mitochondria in the terminal step of the heme biosynthesis pathway.[1,2] FECH inserts reduced ferrous iron into protoporphyrin (PPIX) to produce proto-heme IX. Loss of FECH activity thus leads to reduced heme production, accompanied by accumulation of substrate PPIX. Many intermediates of heme synthesis are porphyrins, known for diseases of porphyria caused due to defects in the synthesis pathway.[3] In humans, diminished FECH activity is associated with erythropoietic protoporphyria (EPP), characterized by buildup of PPIX in erythrocytes. The main symptom of EPP is photosensitization of skin, with mild anemia and liver damage in some cases.[4]

Fech^{m1Pas} mice have been used as a mouse model for EPP.[5] They carry a point mutation in the *Fech* gene, causing partial loss of *Fech* activity and PPIX accumulation. This autosomal recessive inherited defect is due to a T to A transversion mutation at nucleotide 293, leading to a methionine to lysine substitution at position 98 of the *Fech* gene, causing reduced enzyme activity compared to the wild-type (WT) mice. The mutation in the gene was generated in a chemical mutagenesis experiment using ethylnitrosourea during inbreeding of mice. Heterozygous mutants are phenotypically normal and exhibit close to 65% to 70% *Fech* activity without any pathologic abnormalities.[6] *Fech*^{m1Pas} homozygotes, however, have less than 6% to 7% *Fech* activity and

show age-dependent cutaneous photosensitivity and jaundice, with hepatotoxicity.[7] Mice with complete loss of *Fech* are embryonically lethal.[8]

We have previously described how FECH and thus heme are involved in ocular neovascularization.[9–11] We showed that *Fech*^{m1Pas} mice, both homozygotes and heterozygotes, had reduced lesions in the laser-induced choroidal neovascularization (L-CNV) model.[9] In the oxygen-induced retinopathy (OIR) model, again heterozygous and homozygous *Fech*^{m1Pas} mice showed a significant reduction in retinal neovascularization and vaso-obliteration compared to age-matched WT animals, with markedly diminished vascular cell proliferation in the retina.[10] FECH is expressed at varying levels in all normal cell types (highest in erythroid cells, then endothelium; http://biogps.org/#goto=genereport&id=2235). However, it was overexpressed in and around neovascular lesions in the L-CNV and OIR models, as well as in eyes from human patients with wet age-related macular degeneration.[9–11]

The antifungal drug griseofulvin, with a known off-target effect against FECH, also showed similar reductions in neovascularization after intravitreal administration in OIR and L-CNV mice.[9,10] Knockdown of *Fech* in the eye, using an siRNA approach, plus *Fech* inhibition with novel small molecules (Lambert-Cheatham NA, et al. *IOVS* 2020;61:ARVO E-Abstract 3978), caused a significant reduction of neovascular lesions in the L-CNV model. Acute inhibition of *Fech* in vivo using a chemical analog of PPIX, *N*-methyl protoporphyrin (NMPP),[12] markedly decreased mitochondrial bioenergetics of the retina and caused a selective dysfunction in cytochrome *c* oxidase of the electron transport chain.[11]

The molecular mechanism studies underlying some of the pathologic characteristics of FECH-deficient mice have been heavily focused on EPP, liver diseases, and now pathologic angiogenesis.[4,6,9,10,13] However, the ocular phenotype of these mutant mice remains uncharacterized. While it is clear that *Fech* deficiency in mice reduces neovascularization, *Fech*^{m1Pas} retinal physiology in the absence of neovascular stimulus has not been explored.

Our goal was to thoroughly characterize the ocular features of *Fech*-deficient mice. We assessed retinal structure, PPIX, vasculature, visual activity, and bioenergetic phenotypes of *Fech*^{m1Pas} homozygous, heterozygous, and WT littermates. Such characterization will be useful for the further study of heme deficiency in retinal and choroidal angiogenesis.

Methods

Animals

Animal experiments were approved by the Indiana University School of Medicine Institutional Animal Care and Use Committee, and experiments were performed in adherence to the ARVO Statement for the Use of Animals in Ophthalmic and Vision Research. The *Fech*^{m1Pas} mutant mice on a BALB/c background[6] were purchased from Jackson Laboratory (Bar Harbor, ME, USA) and backcrossed into C57BL/6J for 4 to 5 generations. Mixed-sex littermates from inbred matings at P17, 1 to 2 months, and 6 months were used for experimentation. Mice were anesthetized for all procedures by intraperitoneal injections of 80 mg/kg ketamine hydrochloride and 10 mg/kg xylazine; then, 1% tropicamide solution (to dilate pupils) and hypromellose ophthalmic demulcent solution (to lubricate corneas) (Gonak; Akorn, Lake Forest, IL, USA) were topically administered to eyes prior to imaging. Mice were euthanized by isoflurane overdose followed by cervical dislocation.

Fundoscopy, Protoporphyrin IX Imaging, and Optical Coherence Tomography

Fundus images were captured for each individual eye using a Micron IV intraocular imaging system (Phoenix Research Labs, Pleasanton, CA, USA). All in vivo imaging was done between 9:30 a.m. and 12:30 p.m. on light-adapted mice, housed under standard 12-hour light/dark cycles, although room lights were turned off for fluorescence image capture. Mice were placed on a heated stage and positioned appropriately for acquiring images. PPIX fluorescence (excitation at 403 nm, emission at 628 nm) was measured with a custom bandpass filter set (403/95 and 628/40; Semrock, Rochester, NY, USA). A stock solution of PPIX in a polypropylene tube was used to optimize imaging settings, and then the same exposure and gain settings were used for all PPIX imaging. Retinal layers[14,15] were assessed by optical coherence tomography (OCT) imaging, using the Micron IV system as described.[16] To ensure representative scans, five OCT B-scans were captured per eye: horizontally through the optic nerve head (ONH), then approximately two ONH diameters superior and inferior to the ONH, and then perpendicularly approximately two ONH diameters temporal and nasal to the ONH.

Fluorescein Angiography and Retinal Vessel Quantification

Animals after anesthetization were injected with 25% fluorescein sodium dye (Fisher Scientific, Pittsburgh, PA, USA) in phosphate-buffered saline at 50 µL/25 g body weight. Retinal fundus images were captured 30 seconds after fluorescein administration to allow retinal vessels to fill with the dye.

Avascular area, venous width, and arterial tortuosity were quantified using the publicly available MATLAB program, QuantBV v1.0 (www.quantbv.com), with its associated prevalidated protocol.[17] Background fluorescein saturation in the images was minimized using the contrast and brightness enhancement filter tool in the open-source imaging program Gimp v2.10.14. Avascular area was quantified by uploading the filtered images into QuantBV v1.0. Venous width was quantified using QuantBV v1.0 to average six to eight width measurements along the largest retinal vein at a distance of 0 to 275 ± 25 µm from the optic nerve. Arterial tortuosity refers to the total distance traveled by the artery in two dimensions over the tangent distance traveled. Arterial tortuosity was quantified using QuantBV to calculate tortuosity of the largest artery at a distance of 0 to 175 ± 25 µm from the optic nerve.

Retinal Wholemount Vasculature Staining

The retinal flatmounts were prepared and immunostained as described previously.[10] Briefly, after removal of the optic nerve, the anterior eye parts, and lens from the 2-month-old adult mouse eyes, the neural retina was carefully dissected from the RPE-choroid sclera complex and transferred to a glass slide. Four radial incisions were made, from the periphery up to ~2 mm radially distant from the site of the optic

Investigative Ophthalmology & Visual Science

nerve to allow the retina to lie flat for imaging. Individual retinal flatmounts were fixed again in 4% paraformaldehyde overnight at 4°C. After fixation, retinal flatmounts were washed twice in PBS and then permeabilized for 2 hours in blocking buffer containing 0.5% Triton X-100 in 10% BSA prepared in PBS. After incubation, retinal flatmounts were stained over 2 days at 4°C in a shaker and incubated in *Griffonia simplicifolia* isolectin B4 (GS-IB4; biotin conjugated, 1:250 dilution; Invitrogen, Carlsbad, CA, USA; cat. 121414) in 0.5% Triton X-100 in 1% BSA prepared in PBS. After the incubation, retinal flatmounts were washed 4 × 15 minutes in PBS and detection reagent (AlexaFluor-488–streptavidin; 1:400 dilution in 0.5% Triton X-100 in 1% BSA prepared in PBS; Jackson Immunoresearch, West Grove, PA, USA; cat. 016-480-084) was added to each retina and incubated overnight at 4°C. After staining, retinal flatmounts were washed 4 × 15 minutes in PBS. Finally, immunostained retinal flatmounts were transferred to glass slides and coverslipped with Fluoromount-G (Southern Biotechnology, Birmingham, AL, USA) and imaged using confocal microscopy on a Zeiss (Jena, Germany) LSM700.

Retinal Sprouting Assay

An ex vivo murine retinal angiogenesis assay was performed as described previously[9,18] with slight modifications. Briefly, retinal pieces (approximately 1 mm in diameter) were isolated from mice (4–6 weeks old) and placed in PBS. Each retinal piece was collected individually into 48-well plates and embedded in fibrin gel (containing bovine fibrinogen [4 mg/mL], aprotinin [5 µg/µL], and bovine thrombin [500 mU/mL]) in serum-free Dulbecco's modified Eagle's medium (DMEM). The fibrin was allowed to clot for ~20 minutes into a semigel form at 37°C in a CO_2 incubator. Then, DMEM containing 10% FBS and human $VEGF_{165}$ (100 ng/well) was added. The tissue was grown for 3 days at 37°C in a CO_2 incubator, and then the medium was replaced. After day 7, endothelial sprouting was monitored and photographed daily for another 48 hours after initial sprouting. Image analysis of the retinal endothelial sprouting was performed manually using ImageJ software (National Institutes of Health, Bethesda, MD, USA), and length of the newly formed retinal sprouts from the edge of the retinal piece to the distance migrated was quantified in at least four directions at given regions of interest per treatment per time point. Retinal endothelial cell sprouting was represented as sprouting distance in pixels.

Choroidal Sprouting Assay

An ex vivo murine choroidal sprouting assay was performed as described previously[9,19] with slight modifications. Briefly, choroid-sclera was dissected from mice (7–8 weeks old) and cut into small pieces. Choroidal pieces were embedded in Matrigel (growth factor reduced) and grown in EGM-2 complete medium containing essential growth factors, including human VEGF, human FGF, R3-IGF, and human EGF and 5% FBS along with antibiotics for 72 hours to allow sprouting to initiate. Endothelial cell sprouting was monitored and photographed daily for another 48 hours after initial sprouting. Image analysis of the choroidal sprouting was performed manually using ImageJ software, and length of the choroidal endothelial sprout from the edge of the choroidal piece to the distance migrated was quantified in at least four directions at given regions of interest per treatment per time point and choroidal endothelial sprouting represented as the sprouting distance in pixels.

Histologic Analysis

For examining histologic sections of the posterior portion of individual eyes, mice were euthanized at indicated ages, and eyes were enucleated for overnight fixation in 4% paraformaldehyde solution. Eyes were processed for embedding in paraffin and sectioned at 5 µm thickness by the Indiana University School of Medicine Histology Core. Hematoxylin and eosin (H&E) staining was performed and images were captured on an EVOS/fl digital microscope (AMG, Mill Creek, WA, USA) using a 20 × objective. Image brightness and contrast were adjusted in ImageJ. Retinal structure and morphology were assessed. The thickness of retinal layers was determined in ImageJ by measuring the distance in pixels from ganglion cell layer (GCL) to inner nuclear layer (INL) and GCL to outer nuclear layer (ONL), respectively. To determine alterations to these layers, the ratio of this distance was calculated. Additionally, we assessed layer thickness by manually counting the number of rows of nuclei making up the three respective nuclear layers as described.[10,16] Four measurements were taken per eye (either side of the optic nerve on two pupillary–optic nerve sections each) and averages reported; representative images are presented aligned along Bruch's membrane as described.[14,15]

Electroretinogram

Electroretinogram (ERG) was measured using an electrodiagnostic LKC system (UTAS-E 2000; LKC Technologies, Gaithersburg, MD, USA) to assess the function of the retina. Mice were dark adapted overnight before taking measurements for scotopic a-wave and b-wave responses.[10,16] Scotopic rod measurements were recorded following white light flashes of increasing intensities of 0.025, 0.25, and 2.5 log cd·s/m^2, at time intervals of 10, 20, and 30 seconds. For measurement of photopic cone responses, mice were light adapted to a white background for 10 minutes, followed by flashes of light stimulation at 0, 5, 10, and 25 log cd·s/m^2 intensities. The trace amplitude between time 0 and the lowest point on the trace was considered the a-wave, and the amplitude between the lowest trace and the highest peak following oscillatory potentials was considered the b-wave.

Optomotor Response

To evaluate the visual acuity, we used a computer-based optomotor response (OMR) test (OptoMotry 1.7.7; Cerebral Mechanics, Lethbridge, Alberta, Canada) as described earlier.[20] In brief, free moving mice were tested for visual acuity by observing head movements that track rotating sinusoidal gratings. These observations were made in real time, via a video camera projecting to the computer screen. The observer was masked to the genotype of mice. Mice were placed on the platform and allowed to settle for 5 minutes. In the rotating virtual drum, spatial frequency at 100% contrast was systematically increased in the staircase method until the mice were unable to track them. The highest spatial frequency each eye could track is reported as a measure of visual acuity.

Investigative Ophthalmology & Visual Science

Retinal Mitochondrial Bioenergetics

For retinal ex vivo oxygen consumption rate (OCR) measurements, protocols were adapted as previously described.[11,21,22] Briefly, eyes were enucleated and the retina was isolated from the posterior cup. Retinal punches (1 mm diameter) were dissected from an area adjacent to the optic nerve to minimize variability in retinal thickness. Retinal punches were incubated in Seahorse XF DMEM pH 7.4 containing 5 mM HEPES (Agilent, Santa Clara, CA, USA) supplemented with 12 mM glucose and 2 mM L-glutamine for 1 hour in a room air incubator at 37°C. For OCR measurement, 0.5 µM carbonyl cyanide-4-(trifluoromethoxy)phenylhydrazone (FCCP) (to collapse the mitochondrial proton gradient, allowing maximal respiration determination) and 0.5 µM rotenone/antimycin A (to block mitochondrial complexes I and III, allowing determination of nonmitochondrial respiration) were injected, and OCR was determined. All Seahorse kinetic traces were analyzed using Wave 2.4 software (Agilent, Santa Clara, CA, USA).

Statistical Analysis

Comparisons between groups were performed using GraphPad Prism v. 8 (GraphPad Software, La Jolla, CA, USA) with one-way ANOVA with Tukey's post hoc tests as indicated. P values <0.05 were considered statistically significant. Means ± SEMs are shown for all graphs unless indicated otherwise; n is listed in figure legends.

Results

Fech^{m1Pas} Homozygotes Have Pronounced PPIX Buildup in the Retina

We evaluated retinal structure in vivo using fundus images and OCT and captured images of retinal layers from anesthetized mice at postnatal day 17 (P17), 2 months, and 6 months of age (Fig. 1, Supplementary Fig. S1, and Supplementary Fig. S2). No abnormalities were found in the retinal structure of heterozygous and homozygous *Fech*^{m1Pas} mice compared with WT littermates (Figs. 1A, 1C, Supplementary Figs. S1A, S1C, S2A, S2C). In order to assess the presence of FECH substrate PPIX in retinas, we evaluated PPIX fluorescence. PPIX fluorescence was detected throughout the retina but notably in the retinal vessels at P17 and was continually detected in adult retinas (2, 6 months) of *Fech*^{m1Pas} homozygotes, with no detectable PPIX buildup observed in WT and heterozygous animals (Fig. 1B, Supplementary Figs. S1B, S2B).

Retinal Vasculature Shows No Abnormalities or Vascular Leakage

We assessed vascular leakage in the *Fech*^{m1Pas} mice by fluorescein angiography. Retinal vessels showed no pathologic signs of leakage (Fig. 2A). Additionally, we quantified retinal vessel dimensions to determine avascular area, vessel width, and tortuosity and found no significant changes (Fig. 2B). In order to further investigate defects in the retinal vasculature of *Fech*^{m1Pas} mice, we examined retinal flatmounts of 2-month adult littermates stained with GS-IB4. Adult retinas (2 months old) from *Fech*^{m1Pas} mice did not show any signs of pathology (Fig. 2C, Supplementary Fig. S3)

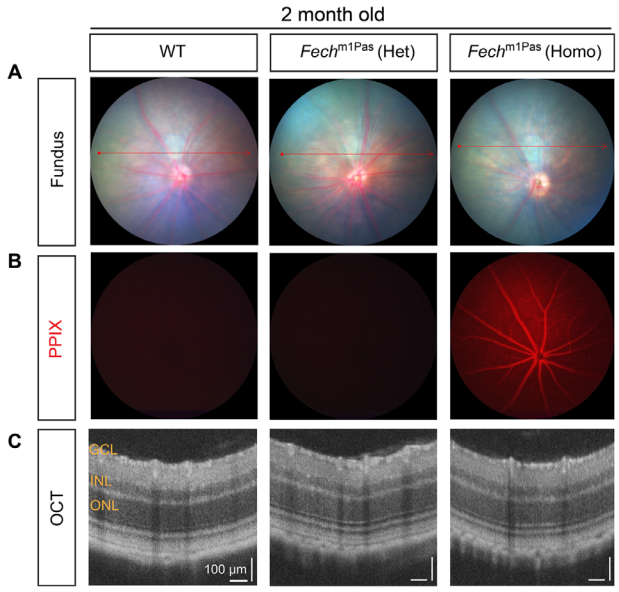

Figure 1. In vivo ocular imaging of adult *Fech*^{m1Pas} mutant mice. (**A**) Representative fundus photographs of 2-month-old *Fech*^{m1Pas} homozygous (Homo) and heterozygous (Het) mutants and WT animals (the *white halo* seen close to optic nerve head is an artifact). (**B**) PPIX fluorescence imaging. (**C**) OCT images from adult *Fech*^{m1Pas} mutant and WT animals from the plane indicated in the fundus photograph (*red lines* in **A**). Representative data from n = 8–12 eyes, n = 4–6 animals per genotype.

in any vascular plexus. Likewise, fluorescein angiography of aged (6-month-old) mice did not reveal any pathology (Supplementary Fig. S2D).

Fech Mutation Reduces Retinal and Choroidal Sprouting Ex Vivo

VEGF[23,24] is one of the major stimulants for both retinal and choroidal neovascularization.[25] We have shown previously that FECH depletion suppresses VEGF-mediated signaling via endothelial nitric oxide synthase (eNOS) and hypoxia-inducible factor-1 (HIF-1) in human retinal endothelial cells.[9] Hence, we investigated the consequences of *Fech* deficiency on VEGF-mediated angiogenesis using retina and choroid ex vivo angiogenesis assays in *Fech*^{m1Pas} mutants. In the retina sprouting assay, treatment with recombinant VEGF greatly stimulated sprouting in WT retina, but reduced endothelial outgrowth was observed in heterozygous and homozygous *Fech*^{m1Pas} mutants (Fig. 3A). Quantification confirmed that FECH deficiency significantly reduced the VEGF-mediated retinal sprouting compared to the WT control (Fig. 3B). Furthermore, in the choroidal sprouting assay, homozygous *Fech*^{m1Pas} mutation decreased sprouting compared to the WT controls, but this was not seen with heterozygous *Fech*^{m1Pas} mutant tissue (Fig. 3C). Quantification of the endothelial sprouts confirmed that homozygous *Fech*^{m1Pas} mutation significantly diminished the choroidal sprouting (Fig. 3D).

Fech^{m1Pas} Mice Show No Abnormalities in Individual Retinal Layers

In order to assess changes in the retinal tissue and individual retinal layers, we investigated H&E-stained retinal

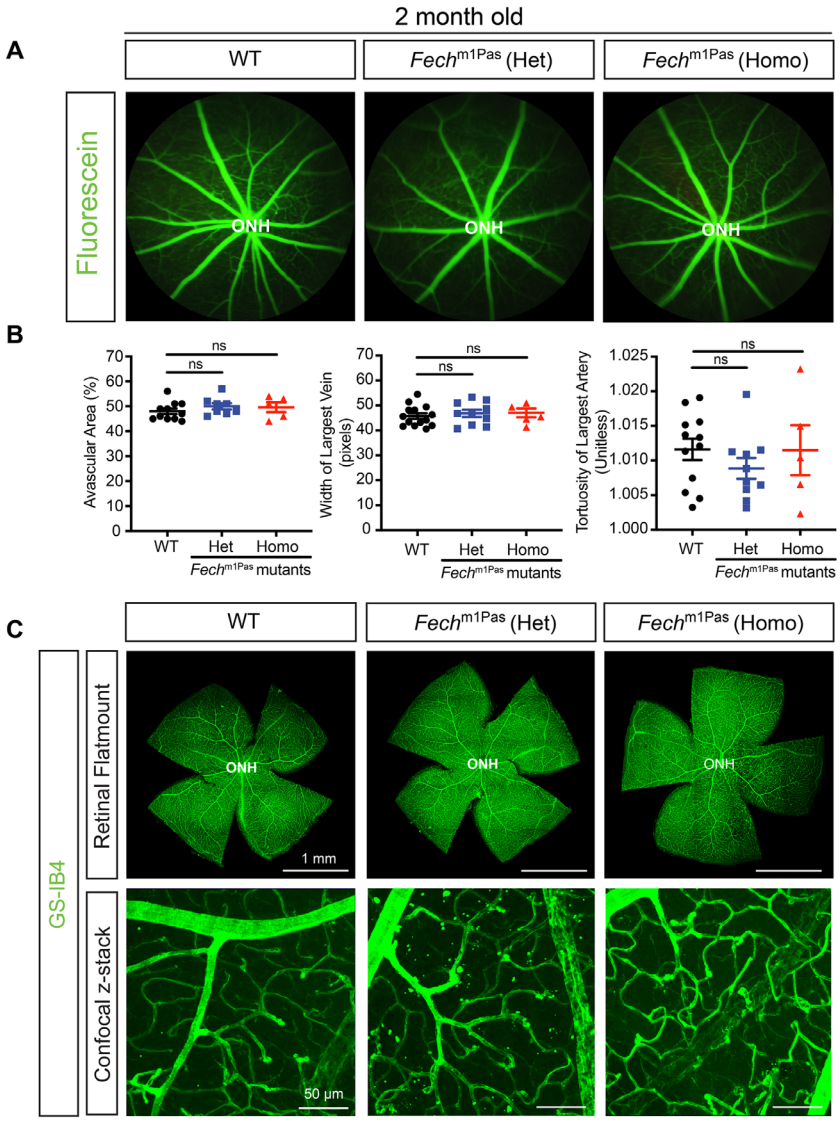

Figure 2. Vascular organization in adult *Fech*^{m1Pas} mutants. (**A**) Fluorescein angiography images of 2-month-old *Fech*^{m1Pas} homozygous (Homo) and heterozygous (Het) mutants and WT animals. Vasculature shown in *green*; $n = 6$–12 eyes, $n = 3$–6 animals. (**B**) QuantBV vessel analysis of fluorescein angiography. Data represented as mean ± SEM, $n = 5$–12 eyes, $n = 3$–6 animals; ns, nonsignificant (one-way ANOVA). (**C**) Confocal overview of retinal flatmounts from *Fech*^{m1Pas} mutants and WT animals stained with GS-IB4 (*green*; labels vasculature) and confocal Z-stack merged images, $n = 4$–6 retinas, $n = 3$–6 animals per group. Note that punctate staining in the high-magnification image from the heterozygote is artifactual. ONH, optic nerve head.

sections of littermates from WT, heterozygous, and homozygous *Fech*^{m1Pas} mice at 2 and 6 months of age (Fig. 4, Supplementary Fig. S4). Qualitative analysis showed no morphologic changes (Fig. 4A, Supplementary Fig. S4A). Quantification of retinal thickness showed no signs of retinal thinning in all three genotypes (Fig. 4B, Supplementary Fig. S4B). We also evaluated the number of individual rows of nuclei making up the GCL, INL, and ONL. Number of nuclei in the respective layers did not show any changes between the littermates (Figs. 4C–E, Supplementary Figs. S4C–E).

Fech^{m1Pas} Mice Had Normal Retinal Function and Optomotor Reflexes

Next, we evaluated the function of the neural retina in *Fech*^{m1Pas} mice using ERG. Dark-adapted mice were stimulated with light flashes and scotopic and photopic responses were recorded (Fig. 5A). Scotopic a-wave corresponding to the activity of rod photoreceptor cells showed no changes across the three genotype groups (Fig. 5B). Similarly, b-waves depicting bipolar cell activity for both scotopic and photopic vision showed no defects among the three genotypes (Figs. 5C, 5D). We also evaluated visual acuity of *Fech*^{m1Pas} mice, assessing OMR in response to moving light and dark patterns. There was no significant difference between the spatial frequency threshold among all three genotypes of *Fech*^{m1Pas} mice (Fig. 5E).

Retinal Bioenergetics of *Fech*^{m1Pas} Mice Do Not Vary by Genotype

Fech inhibition using chemical inhibitor NMPP led to mitochondrial dysfunction in murine retina by decreasing

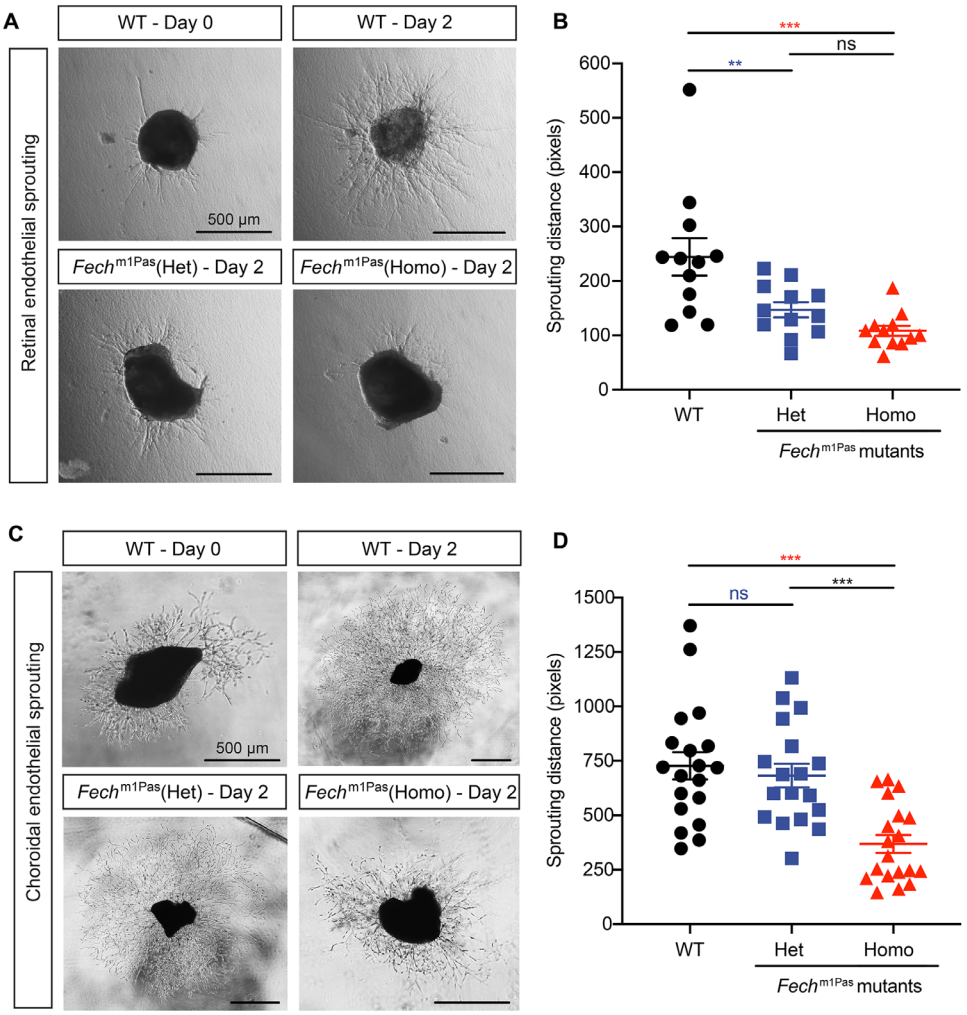

Figure 3. *Fech*^{m1Pas} mutant inhibits retinal and choroidal sprouting ex vivo. (**A**) Representative phase-contrast images of retinal sprouts from *Fech*^{m1Pas} homozygous (Homo) and heterozygous (Het) mutants and WT animals formed after 48 hours of VEGF treatment. (**B**) Quantification of sprouting distance from the edge of the retinal tissue to the end of the sprouts averaged from four perpendicular directions using ImageJ software. Data represented as mean ± SEM, $n = 12$ retinal pieces per treatment; $n = 5$–6 eyes, ns, not significant, $^{**}P < 0.01$, $^{***}P < 0.001$ (ANOVA with Tukey's post hoc test). (**C**) Representative phase-contrast images of choroidal sprouts from *Fech*^{m1Pas} mutants and WT controls formed after 48 hours of VEGF treatment. (**D**) Quantification of choroidal sprouting distance from the edge of the choroidal tissue to the end of the sprouts averaged from four perpendicular directions using ImageJ software. Data represented as mean ± SEM, $n = 18$–19 choroidal pieces per treatment, $n = 8$–10 eyes; ns, nonsignificant, $^{***}P < 0.001$ (ANOVA with Tukey's post hoc test).

oxidative phosphorylation, ATP production, and reduced cytochrome *c* oxidase expression.[11] We further sought to characterize mitochondrial bioenergetics of retinal tissue from *Fech*^{m1Pas} mice and establish a baseline OCR of oxidative phosphorylation (Fig. 6A). OCR corresponding to basal respiration showed comparable mitochondrial function in all three genotypes (Fig. 6B). FCCP uncoupler at a 0.5-µM concentration was used to collapse the potential gradient and measure maximal activity of the electron transport chain (ETC). There was no change observed in FCCP-induced maximal respiration in the littermates (Fig. 6C). Similarly, OCR linked to spare respiratory capacity, as identified by rotenone and antimycin administration, showed no change between WT, heterozygous, and homozygous *Fech*^{m1Pas} mice (Fig. 6D).

Discussion

Loss of FECH activity has been associated with several physical abnormalities, but the role of deficient FECH activity in the ocular system remains obscure. There is strong evidence to suggest that heme plays an important role in ocular endothelial biology.[9–11] In the first step toward providing a thorough retinal characterization of heme synthesis enzyme *Fech*, we studied the retinal phenotype of animals with a partial loss-of-function *Fech* mutation. We characterized retinal levels *of Fech* substrate PPIX, retinal morphology and structure, vasculature, visual activity, and mitochondrial function. We also measured ex vivo VEGF-induced angiogenesis of retinal and choroidal tissue.

The *Fech*^{m1Pas} loss-of-function point mutation leads to deficiency in *Fech* activity, with mice homozygous for this

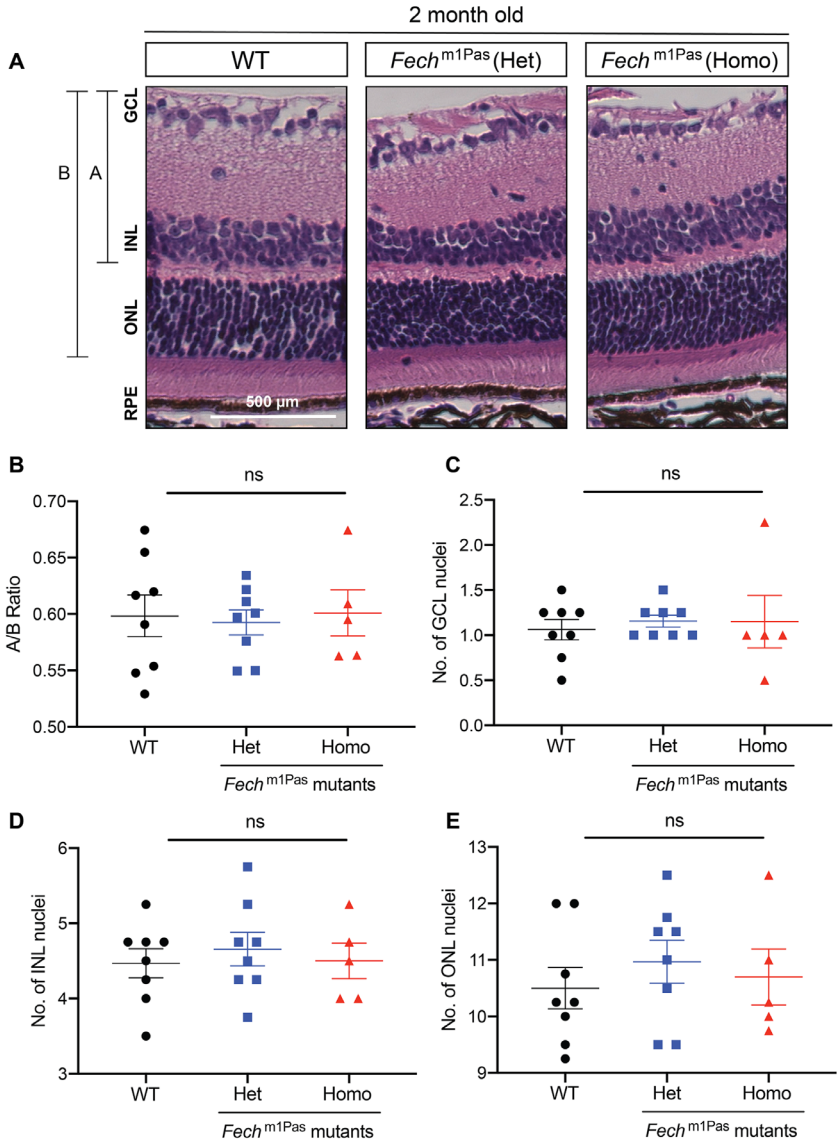

Figure 4. Individual retinal layers of adult *Fech*^{m1Pas} mice are normal. (**A**) Representative images of H&E sections of the retinas of 2-month-old *Fech*^{m1Pas} homozygous (Homo) and heterozygous (Het) mutants and WT animals. (**B**) Quantification of the A/B ratio as indicated. Quantification of the number of rows of nuclei (thickness) making up the (**C**) GCL, (**D**) INL, and (**E**) ONL. Data represented as mean ± SEM, $n = 5$–8 animals per genotype; ns, not significant (one-way ANOVA).

mutation bearing less than 6% activity.[5,6] These *Fech*^{m1Pas} mice display inherited EPP along with mild liver damage and photosensitivity. Deficiency in FECH function leads to accumulation of substrate PPIX and depletion of heme production.[26] Using the intrinsic fluorescence of protoporphyrin, we first confirmed this phenotype by directly assessing PPIX levels in the eyes of juvenile and adult *Fech*^{m1Pas} mice. *Fech*^{m1Pas} homozygotes showed a pronounced buildup of PPIX levels in the retina as early as P17. This was seen in vessels, likely due to systemic PPIX buildup, but also in the surrounding retinal tissue, either from perfusion or local PPIX production. Mice heterozygous for this mutation showed no detectable PPIX fluorescence in the retina, comparable to the WT genotype, although this may reflect limited sensitivity of our detection system as PPIX is known to be moderately increased systemically in *Fech*^{m1Pas} heterozygotes.[6]

Despite the reported phototoxicity of PPIX in vivo observed systemically,[13] *Fech*^{m1Pas} mice showed normal retinal physiology but with PPIX accumulation in the retina. Interestingly, a case report of an EPP patient showed development of idiopathic optic nerve atrophy caused by vascular obstruction and vision loss.[27] It is interesting to speculate whether PPIX buildup coincided with the atrophy in this patient. Perhaps *Fech* mutation could have deleterious effects under conditions of stress, such as sustained intense light exposure. Our new method to assess ocular PPIX in vivo could be used for exploring such questions and potentially be scaled up clinically to noninvasively assess retinas of EPP patients as well.

Adult *Fech* mutant retinas showed no signs of aberration in the blood vessels. Histologically, retinal layers in all three genotypes maintained normal morphology and structure. Nuclei counted in the GCL, INL, and ONL were simi-

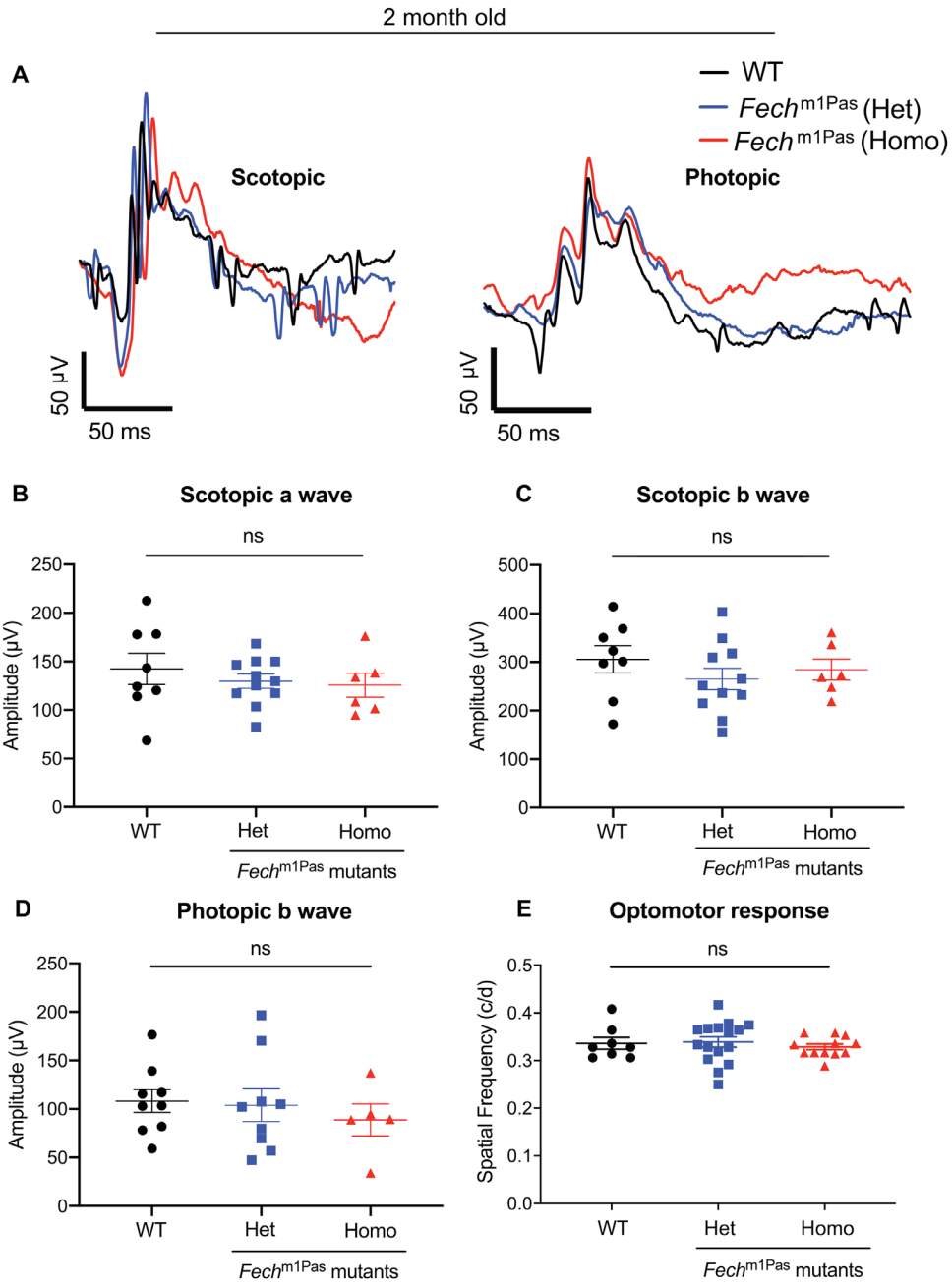

Figure 5. *Fech*^{m1Pas} mice had comparable visual activity and optomotor response. (**A**) Representative mean ERG traces of dark-adapted *Fech*^{m1Pas} homozygous (Homo) and heterozygous (Het) mutants and WT mice. Quantification of (**B**) scotopic a-wave, (**C**) scotopic b-wave, and (**D**) photopic b-wave (stimulus: scotopic = 2.5, photopic = 25 cd·s/m^2). (**E**) Quantification of the optomotor response of mice from each genotype. Data represented as mean ± SEM, n = 6–11 animals; each data point corresponds to mean of left and right eye. ns, not significant (one-way ANOVA).

lar in all three genotypes, showing no signs of retinal thinning, degeneration, or detachment of RPE. This is supported by our observations with ERG recordings, showing healthy retinal function. For the first time, visual function and behavior of mice with a loss-of-function *Fech* mutation are documented. We did not find any abnormalities in the neural retinal activity, suggesting no defect in the physiologic response to light stimuli and conduction of action potential through the inner retina. OMR to moving light patterns showed no abnormality in visual behavior. Thus, despite the reported cutaneous phototoxicity of PPIX in vivo,[13] *Fech*^{m1Pas} mice showed normal retinal physiology. This corroborates our previous findings with the FECH-inhibiting drug griseofulvin, which shows a therapeutic reduction of retinal and choroidal neovascularization, without causing retinal toxicity.[9,10]

Since FECH depletion reduces pathologic ocular angiogenesis[9,10] but *Fech* mutation did not greatly impact normal vasculature and morphology, we explored whether *Fech* deficiency led to changes in ex vivo angiogenesis (reminiscent of human neovascular pathology) using endothelial cell sprouting assays. These assays allow selective growth of endothelial cells out of retinal[18] and choroidal[19] pieces, which maintain morphology during short-term culture.[28]

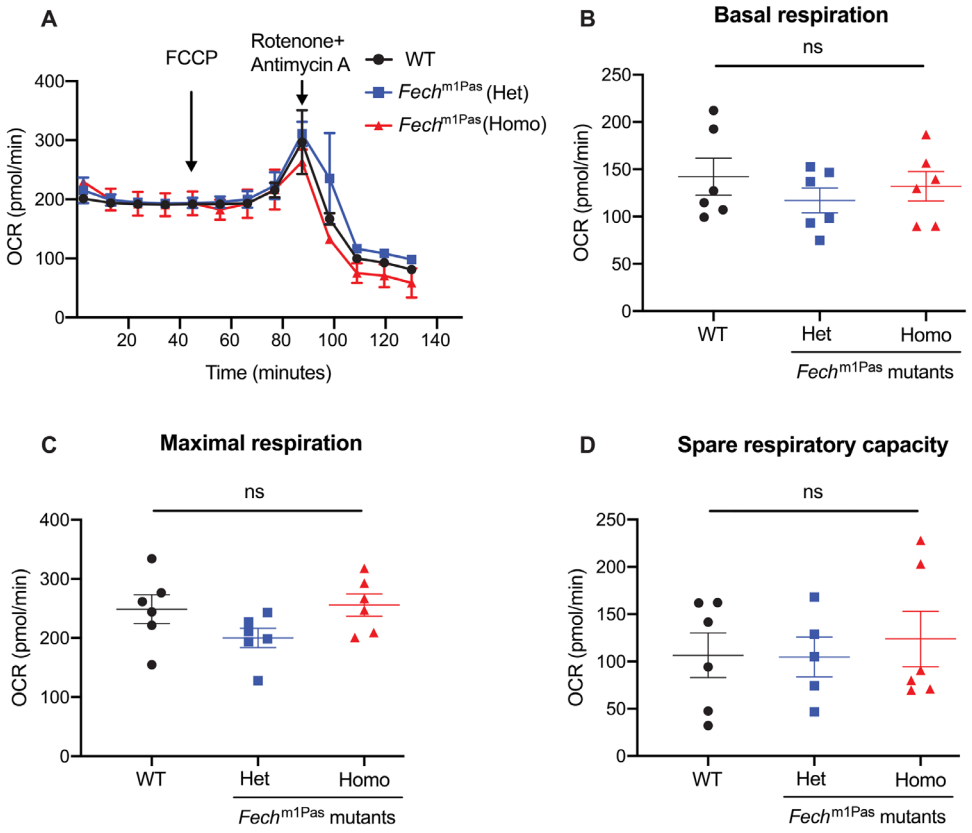

Figure 6. Retinal bioenergetics of *Fech*^{m1Pas} mice do not vary by genotype among littermates. (**A**) Representative OCR kinetic traces for retinas from *Fech*^{m1Pas} homozygous (Homo) and heterozygous (Het) mutants and WT mice. (**B**) Basal respiration, (**C**) maximal respiration, and (**D**) spare respiratory capacity were calculated based on OCR curves for the respective treatment groups. Graphs indicate mean ± SEM, $n = 6$ animals per genotype; each data point corresponds to mean of two tissue punches from each retina. ns, not significant (one-way ANOVA).

Fech^{m1Pas} homozygous mice showed a marked reduction in the ability to form endothelial sprouts from retinal and choroidal explants. This indicates that while the adult vasculature remains grossly normal, pathologic angiogenesis stimulated by VEGF is altered and requires *Fech* activity.

Last, constitutive reduction of FECH activity did not result in an aberration of retinal mitochondrial oxidative phosphorylation. This is consistent with observations in other tissues: no change was seen in the activity of hepatic mitochondrial complexes of *Fech*^{m1Pas} mice in the C57Bl/6J background,[29] although *Fech*^{m1Pas} mice on a BALB/cJ background showed increased activity of respiratory ETC enzymes complex I, III, and IV in the liver. However, we previously found that acute inhibition of *Fech* in vivo results in a significant reduction of mitochondrial respiration and COX IV levels.[11] Thus, a constitutive decrease in *Fech* possibly masks a mitochondrial respiratory defect. Moreover, an inherent point mutation and further backcrossed breeding may have contributed to metabolic compensation in the *Fech*^{m1Pas} mice. Mouse models of metabolic disorders generated from spontaneous mutations, as in the case of *Fech*^{m1Pas} mice, often make up for reduced cellular activity in subsequent generations.[30] A conditional *Fech* mutant, specifically in the retinal and/or choroidal endothelial cells (which have high *Fech* expression), may address the effect of heme depletion directly on mitochondrial activity and overcome the problem of metabolic compensation.

The retinal structure, activity, and vasculature in *Fech*^{m1Pas} mice are largely normal, even with the buildup of PPIX. However, ex vivo endothelial sprouting and pathologic angiogenesis[9,10] appear to be defective in both heterozygotes and homozygotes. This suggests that FECH loss has a more profound effect on pathologic endothelial cell proliferation than physiologic angiogenesis. In the absence of an angiogenic stimulus, FECH deficiency does not seem to affect existing vasculature, which could be an advantage from a therapeutic perspective for future FECH-targeting drugs. The *Fech*^{m1Pas} animals can therefore also be used for assessing the role of FECH specifically in pathologic angiogenesis, as the preexisting vessels were found to be physiologically normal. In conclusion, while some hepatic and porphyrin-related defects are evident in this mouse model, the *Fech*^{m1Pas} mouse offers a promising tool for evaluating the role of heme in neovascularization.

Acknowledgments

Assisted by the Histology Core of the Indiana Center for Musculoskeletal Health at IU School of Medicine and the Bone and Body Composition Core of the Indiana Clinical Translational

Sciences Institute (CTSI) and the Angio BioCore (ABC) at the Indiana University Simon Comprehensive Cancer Center.

Supported by NIH/NEI R01EY025641 and BrightFocus Foundation Macular Degeneration Research Grant M2019069.

Disclosure: **S.P.B. Sardar Pasha**, 62/837,506 (P); **T. Shetty**, None; **N.A. Lambert-Cheatham**, None; **K. Sishtla**, None; **D. Mathew**, None; **A. Muniyandi**, None; **N. Patwari**, None; **A.D. Bhatwadekar**, None; **T.W. Corson**, 15/009,339, 62/837,506 (P)

References

1.. Dailey HA, Meissner PN. Erythroid heme biosynthesis and its disorders. *Cold Spring Harb Perspect Med*. 2013;3:a011676.
2. Shetty T, Corson TW. Mitochondrial heme synthesis enzymes as therapeutic targets in vascular diseases. *Front Pharmacol*. 2020;11:1015.
3. Bonkovsky HL, Guo JT, Hou W, Li T, Narang T, Thapar M. Porphyrin and heme metabolism and the porphyrias. *Compr Physiol*. 2013;3:365–401.
4. Rufenacht UB, Gouya L, Schneider-Yin X, et al. Systematic analysis of molecular defects in the ferrochelatase gene from patients with erythropoietic protoporphyria. *Am J Hum Genet*. 1998;62:1341–1352.
5. Boulechfar S, Lamoril J, Montagutelli X, et al. Ferrochelatase structural mutant (*Fech*^{m1Pas}) in the house mouse. *Genomics*. 1993;16:645–648.
6. Tutois S, Montagutelli X, Da Silva V, et al. Erythropoietic protoporphyria in the house mouse: a recessive inherited ferrochelatase deficiency with anemia, photosensitivity, and liver disease. *J Clin Invest*. 1991;88:1730–1736.
7. Abitbol M, Bernex F, Puy H, et al. A mouse model provides evidence that genetic background modulates anemia and liver injury in erythropoietic protoporphyria. *Am J Physiol Gastrointest Liver Physiol*. 2005;288:G1208–G1216.
8. Magness ST, Maeda N, Brenner DA. An exon 10 deletion in the mouse ferrochelatase gene has a dominant-negative effect and causes mild protoporphyria. *Blood*. 2002;100:1470–1477.
9. Basavarajappa HD, Sulaiman RS, Qi X, et al. Ferrochelatase is a therapeutic target for ocular neovascularization. *EMBO Mol Med*. 2017;9:786–801.
10. Pran Babu SPS, White D, Corson TW. Ferrochelatase regulates retinal neovascularization. *FASEB J*. 2020;34:12419–12435.
11. Shetty T, Sishtla K, Park B, Repass MJ, Corson TW. Heme synthesis inhibition blocks angiogenesis via mitochondrial dysfunction. *iScience*. 2020;23:101391.
12. Shi Z, Ferreira GC. Modulation of inhibition of ferrochelatase by N-methylprotoporphyrin. *Biochem J*. 2006;399:21–28.
13. Libbrecht L, Meerman L, Kuipers F, Roskams T, Desmet V, Jansen P. Liver pathology and hepatocarcinogenesis in a long-term mouse model of erythropoietic protoporphyria. *J Pathol*. 2003;199:191–200.
14. DeRamus ML, Stacks DA, Zhang Y, Huisingh CE, McGwin G, Pittler SJ. GARP2 accelerates retinal degeneration in rod cGMP-gated cation channel beta-subunit knockout mice. *Sci Rep*. 2017;7:42545.
15. Soukup P, Maloca P, Altmann B, Festag M, Atzpodien EA, Pot S. Interspecies variation of outer retina and choriocapillaris imaged with optical coherence tomography. *Invest Ophthalmol Vis Sci*. 2019;60:3332–3342.
16. Sulaiman RS, Merrigan S, Quigley J, et al. A novel small molecule ameliorates ocular neovascularisation and synergises with anti-VEGF therapy. *Sci Rep*. 2016;6:25509.
17. Mezu-Ndubuisi OJ. In vivo angiography quantifies oxygen-induced retinopathy vascular recovery. *Optom Vis Sci*. 2016;93:1268–1279.
18. Rezzola S, Belleri M, Ribatti D, Costagliola C, Presta M, Semeraro F. A novel ex vivo murine retina angiogenesis (EMRA) assay. *Exp Eye Res*. 2013;112:51–56.
19. Shao Z, Friedlander M, Hurst CG, et al. Choroid sprouting assay: an ex vivo model of microvascular angiogenesis. *PLoS One*. 2013;8:e69552.
20. Prusky GT, Alam NM, Beekman S, Douglas RM. Rapid quantification of adult and developing mouse spatial vision using a virtual optomotor system. *Invest Ophthalmol Vis Sci*. 2004;45:4611–4616.
21. Joyal JS, Sun Y, Gantner ML, et al. Retinal lipid and glucose metabolism dictates angiogenesis through the lipid sensor Ffar1. *Nat Med*. 2016;22:439–445.
22. Kooragayala K, Gotoh N, Cogliati T, et al. Quantification of oxygen consumption in retina ex vivo demonstrates limited reserve capacity of photoreceptor mitochondria. *Invest Ophthalmol Vis Sci*. 2015;56:8428–8436.
23. Stahl A, Connor KM, Sapieha P, et al. The mouse retina as an angiogenesis model. *Invest Ophthalmol Vis Sci*. 2010;51:2813–2826.
24. Witmer AN, Vrensen GF, Van Noorden CJ, Schlingemann RO. Vascular endothelial growth factors and angiogenesis in eye disease. *Prog Retin Eye Res*. 2003;22:1–29.
25. Smith LE, Kopchick JJ, Chen W, et al. Essential role of growth hormone in ischemia-induced retinal neovascularization. *Science*. 1997;276:1706–1709.
26. Brady AM, Lock EA. Inhibition of ferrochelatase and accumulation of porphyrins in mouse hepatocyte cultures exposed to porphyrinogenic chemicals. *Arch Toxicol*. 1992;66:175–181.
27. Tsuboi H, Yonemoto K, Katsuoka K. Erythropoietic protoporphyria with eye complications. *J Dermatol*. 2007;34:790–794.
28. Alarautalahti V, Ragauskas S, Hakkarainen JJ, et al. Viability of mouse retinal explant cultures assessed by preservation of functionality and morphology. *Invest Ophthalmol Vis Sci*. 2019;60:1914–1927.
29. Navarro S, Del Hoyo P, Campos Y, et al. Increased mitochondrial respiratory chain enzyme activities correlate with minor extent of liver damage in mice suffering from erythropoietic protoporphyria. *Exp Dermatol*. 2005;14:26–33.
30. Kennedy AJ, Ellacott KL, King VL, Hasty AH. Mouse models of the metabolic syndrome. *Dis Model Mech*. 2010;3:156–166.